Kinetics of Cu Underpotential Deposition on Iodine-Modified Au(111) Electrodes

Alejandro Martínez-Ruíz*

Facultad de Ciencias, Universidad Autónoma de Baja California, A.P. 1820, 22800 Ensenada, B.C., México

Manuel Palomar-Pardavé[†]

Departamento de Materiales, Universidad Autónoma Metropolitana-Azcapotzalco, A.P. 16-306, C.P. 02200 México, D.F., México

J. Valenzuela-Benavides[‡] **and Mario H. Farías**[§]

Centro de Ciencias de la Materia Condensada de la UNAM, A.P. 2681, 22800 Ensenada, B.C., México

Nikola Batina[||]

Departamento de Química, Universidad Autónoma Metropolitana-Iztapalapa, A.P. 55-534, 09340 México, D.F., México

Received: October 11, 2002; In Final Form: July 23, 2003

The kinetics of copper underpotential deposition (UPD) on Au(111) previously covered with an iodine adlayer were investigated by means of cyclic voltammetry (CV) and chronoamperometry (CA) techniques in an aqueous solution containing 1 mM $CuSO_4$ and 0.05 M H_2SO_4. Characterization of the deposition process was based on quantitative analysis of the potentiostatic current−time curves recorded during Cu UPD. It was found that the deposition behavior can be well described by a model that involves three types of contributions: (i) a Langmuir-type adsorption process with two different kinds of two-dimensional nucleation mechanisms, (ii) an instantaneous, and (iii) a progressive contribution, the latter two limited by lattice incorporation of adatoms. It is shown that the main effect of the iodine adlayer is to slow the kinetics of Cu UPD when compared to the same process in the absence of an iodine adlayer. Results from CV also reveal a very stable iodine adlayer even after several Cu deposition/stripping cycles, requiring a high positive potential when surface oxidation takes place in order remove it from the Au(111).

1. Introduction

Studies of adsorption of atoms and small molecules onto metal surfaces have played a fundamental role in the understanding of adsorbate surface interactions. In particular, underpotential deposition (UPD) is strongly influenced by both the nature of the substrate and the composition of the electrolyte. One of the most intriguing aspects of UPD is the anion dependence of the observed structures, which derive from coadsorption or preadsorption of the anion and adatom.[1−6] Important progress in this field has been made by using modern in situ techniques for structural characterization, such as scanning tunneling microscopy (STM) and surface diffraction.[7] For instance, it has been demonstrated that the $(\sqrt{3} \times \sqrt{3})$-R30° structural lattice observed for Cu UPD onto bare Au(111) surfaces in a sulfate-containing medium is due to coadsorption of sulfate or bisulfate ions and Cu adatoms.[7−17]

The adsorption of halogens onto different metallic substrates has been especially well studied in ultrahigh vacuum (UHV) and in the more complex electrochemical environment.[18−25] Of the halogens group, iodine exhibits the strongest adsorption for many metals in electrochemical systems, which has led to its use as a passivated protection layer for surfaces after flame annealing. In earlier studies of iodine adsorption on Au(111), it was shown that the iodine adlayer on Au(111) surface exhibits a $(\sqrt{3} \times \sqrt{3})$R30° atomic structure at low potentials, and a rectangular c(p $\times$ $\sqrt{3}$)R30° overlayer, which compresses from $p = 3$ to $p = 2.49$, and rot-hex structure, as the potential is raised.[21,26−31]

To define and characterize the mechanism and kinetics involved in the deposition process in a quantitative way, traditional electrochemical techniques such as current transients measurements can be used. It offers a significant advantage since the obtained data is easily interpreted with the aid of several theoretical models developed for this purpose.[32−39] In the case of a clean Au(111) surface, copper electrodeposition and growth kinetics have been reported, where it was shown that the UPD process can be described by an adsorption stage, accompanied by an instantaneous 2D-nucleation process limited by lattice incorporation of copper adatoms.[38−42] Although several studies have been performed to better understand the influence of coadsorbed Br^- and Cl^- anions with Cu in the overpotential region, iodine has received little attention despite its characteristic strong adsorption. Therefore, the main goal of this paper is the study of Cu underpotential deposition onto I-modified Au(111).

* Corresponding author. Alejandro Martínez-Ruíz. Tel. and Fax: +52-646-174-4560. E-mail: alejandro@uabc.mx.
† E-mail: mepp@correo.azc.uam.mx.
‡ E-mail: valenzue@ccmc.unam.mx.
§ E-mail: mario@ccmc.unam.mx.
|| E-mail: bani@xanum.uam.mx.

10.1021/jp027197x CCC: $25.00
Published on Web 10/01/2003

2. Experimental Section

Chronoamperometry (CA), cyclic voltammetry **(**CV), and STM were employed for the study of copper electrodeposition onto clean Au(111) and iodine-modified Au(111) substrates in an aqueous electrolyte containing 1 mM $CuSO_4$ in 0.05 M H_2SO_4. The electrolyte was carefully deareated for 30 min using pure N_2 gas. All chemicals used were suprapure grade from Merck. Solutions were prepared with ultrapure water (Millipore Milli-Q).

The electrochemical experiments were carried out in a conventional three-electrode cell system, with a platinum wire used as counter electrode and a copper wire for the Cu/Cu^{2+} reference electrode. All potentials are quoted against this reference electrode. For the gold working electrodes, commercially available 200−300 nm thick gold films on high-temperature glass were used (MHS-GmbH, Germany). To prepare the Au(111) electrode surface the gold film was first annealed in a hydrogen flame for 1 min, forming the (111) facets, and cooled in a nitrogen atmosphere. In the case of the I−Au(111) electrode, the annealed films were immersed in 1 mM KI aqueous solution for 3 min. All samples were thoroughly rinsed with pure 0.1 M H_2SO_4 and quickly transferred to the electrochemical cell.

A BAS 100B (Bioanalytical Systems) potentiostat and a PAR 273 (EG&G) potentiostat were used for the CV and CA experiments. A NanoScope III electrochemical STM from Digital Instruments (Veeco Metrology) was used for in-situ imaging using polymer-coated tungsten tips.

3. Results and Discussion

3.1. Cyclic Voltammetry. The surface quality of the flame-annealed Au substrates was checked by performing CV measurements on bare electrodes in a 0.05 M H_2SO_4 + 1 mM $CuSO_4$ solution and the results were compared to those reported in the literature for Cu UPD on well characterized Au(111).[7,38,43,44] A typical voltammogram for Au thin films recorded at a scan rate of 10 mV/s (see Figure 1a) displayed two distinctive deposition peaks (A and B) centered at +0.2 and +0.032 V, respectively, a behavior characteristic of this system. Because of the great similarity of this voltammogram with those reported in the literature and obtained with single-crystal gold electrodes, with this result we confirm that the flame-annealed gold films have a predominantly (111) orientation.

Figure 1b shows a voltammogram for Cu UPD on I-covered Au(111) recorded under the same conditions specified for the bare Au(111) surface. It resembles the voltammogram for Cu UPD on bare Au(111) in the sense that Cu deposition takes place in a two-step process. Two distinct broad reduction peaks are observed before bulk deposition, but shifted toward more negative potentials when compared to Cu on clean Au(111). The first reduction peak is centered around +0.105 V and a second smaller peak at +0.01 V, with their corresponding oxidation peaks. It is important to note that for potentials more positive than +0.2 V before the first UPD peak, the charge-transfer involved is very low, as demonstrated in Figure 2.

In Figure 2 we show the transferred charge as a function of applied potential for Cu deposition onto a Au(111) and an I-modified Au(111) electrode surface. The charge consumed after the first peak is approximately 205 $\mu C/cm^2$, giving a total of 425 $\mu C/cm^2$ at the end of the negative scan for clean Au(111). In the case of I-modified Au(111), the measured amount of charge transferred after the first peak is approximately 330 $\mu C/cm^2$, with a total charge transfer of approximately 380 $\mu C/cm^2$. This is lower than the expected value of 440 $\mu C/cm^2$ calculated for the formation of an epitaxial (1 × 1) Cu layer on an ideal defect-free Au(111) surface and a two-electron-transfer per Cu atom.[38] The difference could be attributed to the presence of surface defects such as grain boundaries not completely eliminated in the gold film during the annealing process.

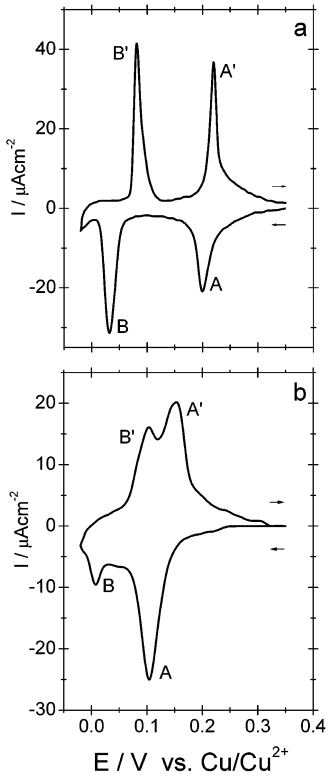

Figure 1. Typical cyclic voltammograms obtained for Cu UPD onto (a) Au(111) and (b) I-modified Au(111) in an aqueous solution containing 1 mM $CuSO_4$ + 0.05 M H_2SO_4. In both cases, the potential was scanned from +0.35 V in the negative direction at a rate of 10 mV/s.

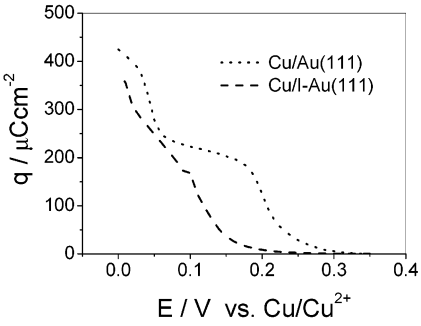

Figure 2. Charge density as a function of applied potential for Cu UPD onto a clean (dotted line) and I-modified (dashed line) Au(111) surface, estimated by integrating the CV curves in Figure 1.

The estimated copper coverage is approximately $\theta_{Cu} = 0.75$ after the first UPD peak and only a small fraction deposited after the second UPD peak for the I-modified surface. This is in strong contrast with the case of a bare Au(111) surface, where 2/3 of a monolayer is deposited after first UPD peak and the remaining 1/3 after the second reduction peak.[14] Apparently sulfate coadsorption is no longer favorable in the presence of an iodine adlayer in order to stabilize the copper structure as in the case for the bare Au(111) surface. This latter point was considered in detail in a recent work from our group.[27]

For more detailed insight into the kinetics of the deposition process, a sequence of cyclic voltammograms were recorded at

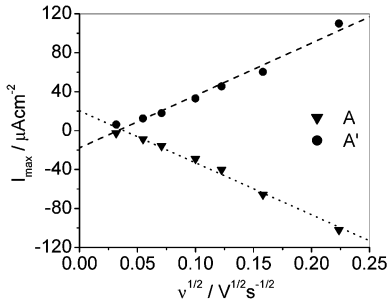

Figure 3. Peaks maxima as a function of the square root of scan rate, for the first deposition (reduction) peak and its corresponding stripping (oxidation) peak, labeled as A and A′, respectively, in Figure 1, for Cu UPD on I-modified Au(111).

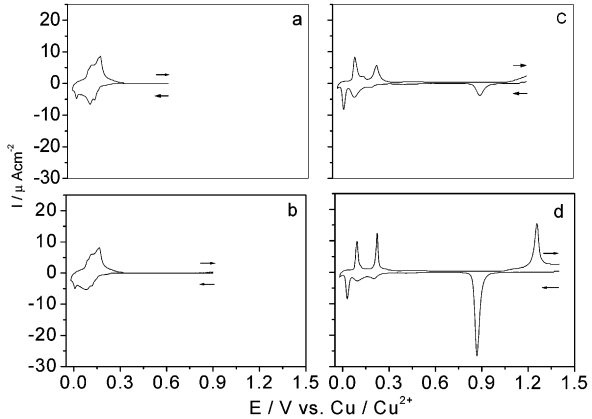

Figure 4. Cyclic voltammograms obtained for Cu UPD onto I-modified Au(111) in an aqueous solution containing 1 mM $CuSO_4$ and 0.05 M H_2SO_4 for different starting potentials E_o: (a) 0.6 V, (b) 0.9 V, (c) 1.2 V, and (d) 1.4 V at a scan rate of 10 mV/s. All scans were initiated in the negative scan direction.

different scan rates (ν) and the current maxima (I_{max}) of the reduction and oxidation peaks measured. Previous studies on the kinetics of Cu UPD onto clean Au(111) have shown this system to be a good example of an instantaneous nucleation and growth process.[32,38] To compare the effect an iodine adlayer has on the deposition mechanism, we first show in Figure 3 the peaks maxima (I_{max}) dependence on the square root of the scan rate. A linear relationship is clearly observed for a wide range of scan rates indicating a diffusion-limited deposition, a result similar to that of Cu UPD on clean Au(111).[38]

Iodine adlayer stability was investigated by performing a series of consecutives CV scans, beginning each one at a higher positive potential. Figure 4 shows cyclic voltammograms taken at four different starting potentials (E_o). For E_o below the gold's oxidation potential the voltammogram in the UPD region resembles that of Cu deposition onto an I-modified Au(111) surface (Figures 4a and 4b). For E_o above the oxidation potential (>1.0 V), partial (Figure 4c) and almost complete removal (Figure 4d) of the iodine adlayer is observed in the UPD region, revealing the characteristic features observed for Cu deposition onto I-free Au surface.

3.2. In-Situ Electrochemical STM. Electrochemical scanning tunneling microscopy (ECSTM) was used to examine the surface morphology of the I-modified Au(111) to ascertain the quality of the substrate and preparation procedure. Immersion of the I-modified Au(111) substrate into the ECSTM cell was done under potential control at +0.35 V, above the first Cu UPD peak. After allowing for thermal drift to settle to an acceptable level, images such as the ones shown in Figure 5 were acquired in large areas of the sample, revealing atomically flat terraces

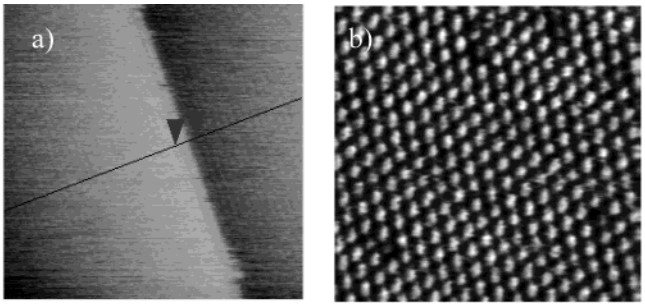

Figure 5. (a) An unfiltered 12 nm × 12 nm ECSTM image of I-modified Au(111) acquired at +0.35 V, with a monatomic step running across the image; (b) an atomically resolved 6 nm × 6 nm image of the iodine adlayer before Cu UPD acquired at the same potential.

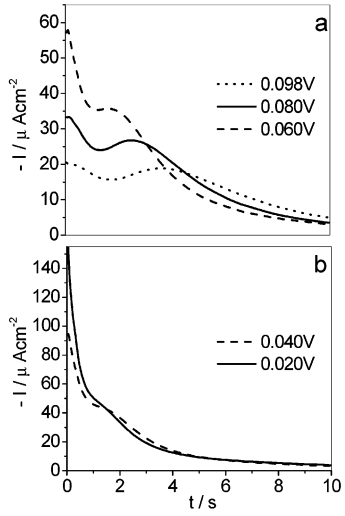

Figure 6. Representative experimental potentiostatic current−time transients recorded during Cu UPD onto I-modified Au(111) from an aqueous solution containing 1 mM $CuSO_4$ and 0.05 M H_2SO_4 for different final potentials**.** In all cases, the potential was first kept at +0.35 V for 20 s, followed by a step to the final values indicated in the figures, i.e., within the potential interval corresponding to (a) the first Cu UPD peak A (see Figure 1b), and (b) the second Cu UPD peak, B.

separated by monatomic steps. After careful measurement of the interatomic distances the expected c(p × √3R-30°) structure was assigned to the image in Figure 5b). A detailed study on the different surface structures observed during Cu UPD on I-modified Au(111) was reported in previous work [27] and will not be addressed here.

3.3. Chronoamperometry. Figure 6 shows a set of current−time curves obtained as a result of stepping the potential to final values within the Cu UPD region, after initially fixing a rest potential of +0.35 V for 20 s. All of these current transients exhibit an initial decay associated with Cu adsorption,[38] followed by a current maximum that shifts to shorter times when the potential step becomes more negative. The general shape of the transients is independent of the final potential as would be expected for a nucleation and growth process. The curves in Figure 6a corresponding to final potential values within the first UPD peak show a well-defined maximum that is less defined for transients with final potential values within the second UPD peak, sometimes masked by the adsorption process (Figure 6b).

To determine the mechanism of nucleation and growth of the Cu UPD process, we analyzed the experimental data by usual procedures.[38] Linearization of the measured transients $I(t)$ for Cu UPD on I-modified Au(111), by either the Cotrell equation

TABLE 1: Parameter Values of Theoretical Transients Used To Fit the Experimental Current Transients Presented in Figure 7 for Cu UPD on I-Modified Au(111)

E (V)	t_m (s)	I_m (μA cm^{-2})	k_1 (μA cm^{-2})	k_2 (s^{-1})	k_3 (μA cm^{-2})	k_4 (s^{-2})	k_5 (μA cm^{-2})	10^3k_6 (s^{-3})
0.098	3.25	18.9	30.2	1.3	8.0	0.04	0.04	0.28
0.080	2.52	26.7	44.2	1.4	15.2	0.08	0.30	2.78
0.060	1.57	35.6	69.2	1.6	25.4	0.13	0.34	2.78
0.040	1.17	44.7	119.2	2.1	38.1	0.21	0.65	5.08
0.020	0.95	51.4	119.2	2.3	32.5	0.21	0.53	6.68

[$I(t) \propto t^{-1/2}$] or by means of an exponential law [$I(t) \propto \exp(-kt)$], yielded nonlinear relationships, indicating the overall process is not diffusion-controlled.

These were then analyzed using the Bewick, Fleischmann, and Thrisk (BFT) theory which was developed to describe 2D growth determined by lattice incorporation of adatoms to the periphery of a growing nucleus and taking into account the overlap of nuclei.[33−35] Within this framework the instantaneous and progressive nucleation are described by

$$I_{2D_i-L_i}(t) = k_3 t \exp(-k_4 t^2) \quad (1)$$

and

$$I_{2D_p-L_i}(t) = k_5 t^2 \exp(-k_6 t^3) \quad (2)$$

respectively. The last contribution to the current transient is due to Cu adsorption (I_{ad}), which may be expressed in terms of a Langmui-type adsorption−desorption equilibrium,[38,47] i.e.,

$$I_{ad} = k_1 \exp(-k_2 t) \quad (3)$$

Here, k_i are constants which depend on several physical parameters determined by fitting the experimental data to the model.[38,47] On this basis the total experimental current transients can be described as the sum of individual contributions, i.e.,

$$I_{total}(t) = I_{ad}(t) + I_{2D_i-L_i}(t) + I_{2D_p-L_i}(t) \quad (4)$$

The nonlinear fitting of eq 4 performed on the current−time curves is shown in Figure 7, with good agreement between our experimental results and the proposed model (for a detailed explanation of the procedure see ref 40). It is seen that current maxima can be associated to an instantaneous 2D nucleation process limited by lattice incorporation of copper adatoms, with small contributions from progressive 2D-nucleation. It is also observed that for all cases Cu UPD is governed by an adsorption process (I_{ad}), followed by a strong instantaneous nucleation $2D_i(I_{2D_i-L_i})$ and a smaller contribution from progressive nucleation $2D_p(I_{2D_p-L_i})$, with the time t_m where the current maxima occurs shifting toward shorter values as the step potential becomes more negative. Table 1 shows the magnitude of each of the fitting parameters k_i which resulted in the best curve fit.

From the contributions of the adsorption and nucleation curves current integration was performed in order to obtain charge density corresponding to each fitted current transient curve. Table 2 shows the charge densities of the three processes contributing to Cu UPD on I-modified Au(111) for each potential step. An increase in the total charge q_{total} can be noted as a function of the potential step E, together with a rapid increase of q_{ad} while there is a slower decrease of $q_{D_i-L_i}$ and $q_{D_p-L_i}$ for more negative step potentials. The porcentage of charge contributed by the adsorption and nucleation processes to the total charge is plotted in Figure 8 as a function of potential step, where the nucleation charge increases at the expense of the adsorption charge. This situation is in contrast with the case

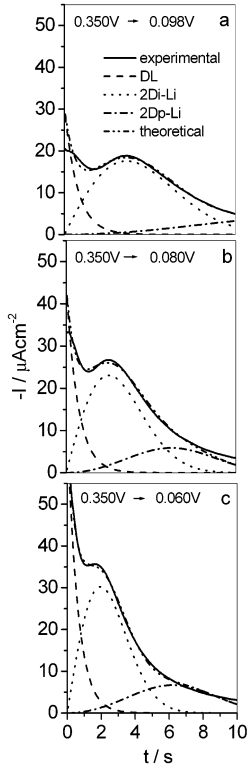

Figure 7. Theoretical nonlinear fits based on eq 4 to the experimental current transients data recorded during Cu UPD on I-modified Au-(111) following a potential step from +0.35 V to different end potentials (a) 0.098 V, (b) 0.080 V, and (c) 0.060 V. Shown in the figure are the individual contributions due to adsorption (dashed line), 2D instantaneous (dotted line) and 2D progressive (dash−dot line) nucleation. The theoretical curve is almost undistinguishable from the experimental curve.

TABLE 2: Charge Densities for Each of the Processes Contributing to Cu UPD on I-Modified Au(111) for the Different Step Potentials Used

E (V)	q_{total} (μC cm^{-2})	q_{DL} (μC cm^{-2})	q_{2Di-Li} (μC cm^{-2})	q_{2Dp-Li} (μC cm^{-2})	$q_{nucleation}$ (μC cm^{-2})
0.098	179.7	23.3	105.2	51.2	156.4
0.080	161.7	30.7	95.4	35.6	131.0
0.060	180.7	42.7	97.6	40.4	138.0
0.040	192.0	56.8	92.8	42.4	135.3
0.020	196.8	73.6	75.5	47.7	123.2

of adsorption and nucleation for Cu UPD on clean Au(111) reported by Hölzle et al.,[38] where the ratio between q_{ad} and $q_{nucleation}$ was found to remain nearly constant for different step potentials. We attribute this difference in behavior to the effect of the iodine adlayer on the deposition process of Cu on Au(111).

Figure 9 shows plots of $\log(I_m)$ and $\log(t_m)$ as a function of potential step. A linear fit to the data yielded slope magnitudes of −5.6 and 7.2, respectively. According to the model used, $(\delta \log I_m/\delta E) \approx -(\delta \log t_m/\delta E)$ was expected.[47] The difference between both values falls within a reasonable difference.

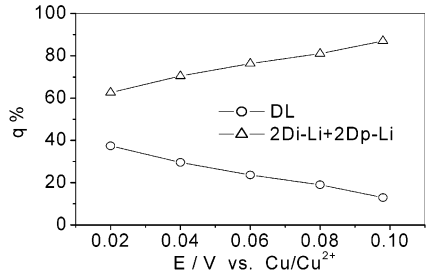

Figure 8. Percentage of charge contribution by the adsorption and nucleation processes for Cu UPD on I-modified Au(111) as a function of step potential.

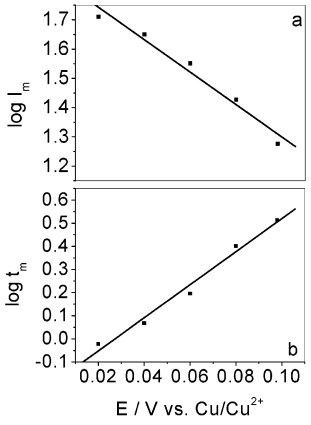

Figure 9. Plots of (a) log I_m and (b) log t_m as a function of potential step for Cu UPD on I-modified Au(111).

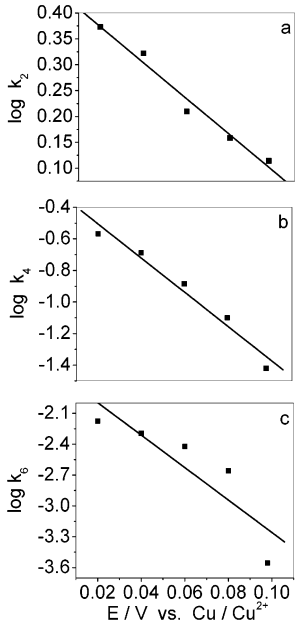

Figure 10. Plots of log k_i for $i = 2$ (panel a), 4 (panel b), and 6 (panel c) as a function of potential step for Cu UPD on I-modified Au(111).

Figure 10a shows a linear fit to a plot of log k_2 versus E , with a slope of -3.49 and a crossing point value of 0.44 at the vertical axis. To explain this result, we use the Butler−Volmer formalism[46] where the adsorption of metallic ions associated with a charge transfer can be described by $k_2 = k_a^\circ \exp[-(1-\beta)zFE/RT]$, which expressed in logarithms takes the form $\log k_2 = \log k_a^\circ - [(1-\beta)zF/2.303RT]E$. This equation represents a straight line in the logarithmic scale with a slope $\delta \log k_2/\delta(-E) = (1-\beta)zF/2.303RT$ and an intercept of log k_a°. Using the above estimated slope, a transfer coefficient β of 0.9 was calculated at a temperature of 298 K. Its closeness to unity suggests an asymmetrical activation barrier and a predominantly reduced species, as hinted by the large potential difference between peak B and B′(see Figure 1b). A β value close to 0.5 is characteristic for metallic deposits on metals. The difference is clearly attributable to the presence of the iodine adlayer on Au(111). The obtained value for k_a° was 2.8 s^{-1}. Figure 10b shows the linear relationship of logk_4 vs potential. The linear fit gives a slope of -12.4. According to the proposed model, the relationship $(\delta \log t_m/\delta E) \approx -1/2(\delta \log k_4/\delta E)$ should be satisfied, so this relationship also confirms the validity of the proposed model with regards to the 2D instantaneous nucleation. Finally, Figure 10c shows the relatioship of the kinetic constant log k_6 (related to 2D progressive nucleation) as a function of E. A linear fit gives a slope of -20.5. Again, the model used establishes the relationship $(\delta \log t_m/\delta E) \approx -1/3(\delta \log k_6/\delta E)$. This relationship also supports the use of the model for 2D progressive nucleation on our data.

4. Conclusions

Cyclic voltammetry (CV) and chronoamperometry (CA) techniques were used to characterized the kinetic mechanism of Cu UPD on I-modified Au(111) in sulfuric acid solution.

From the experimental current transient curves and using the BFT model for nucleation and growth, Cu UPD can be described by an adsorption process followed by two-dimensional instantaneous (2Di-Li)and progressive (2Dp-Li) nucleation and growth processes limited by lattice incorporation of adatoms, in good agreement with recent works for similar systems. It was also found that the potential dependence of adsorption and growth rates follow a Butler−Volmer relation. When compared to previously reported results the kinetics of Cu UPD on I-modified Au(111) are slower than for Cu UPD on clean Au(111). CV results show a highly stable iodine adlayer during the UPD process.

Acknowledgment. A.M.R. gratefully thanks O. M. Aguirre (RIP), C. Carballo, M. Miranda-Hernández, and M. T. Ramírez for their valuable technical assistance. This work was partially supported by CONACyT through projects grants 32158-E and 34132-E and by DCBI-UAMA through project grant 2260220.

References and Notes

(1) Kolb, D. M. *Schering Lecture's Publication*; Schering Research Foundation: Berlin, 1991; Vol. 2, p 1.
(2) Zei, M. S.; Qiao, G.; Lehmpfuhl, G.; Kolb, D. M. *Ber. Bunsen-Ges. Phys. Chem.* **1987**, *91*, 349.
(3) Herrero, E.; Glazier, S.; Abruña, H. D. *J. Phys. Chem. B* **1998**, *102*, 9825.
(4) Möler, F. A.; Magnussen, O. M.; Behm, R. J. *J. Phys. Rev. B* **1995**, *51*, 2484.
(5) Gómez, R.; Yee, H. S.; Bommarito, G. M.; Feliu, J. M.; Abruña, H. D. *Surf. Sci.* **1995**, *335*, 101.
(6) Cavalleri, O.; Gilbert, S. E.; Kern, K. *Surf. Sci.* **1997**, *931*, 377.
(7) Gewirth, A. A.; Niece, B. K. *Chem. Rev.* **1997**, *97*, 1129.
(8) Kleinert, M.; Cuesta, A.; Kibler, L. A.; Kolb, D. M. *Surf. Sci.* **1999**, *430*, L521.
(9) Xu, J. G.; Wang, X. W. *Surf. Sci.* **1998**, *408*, 317.
(10) Zhang, J.; Sung, Y.-E.; Rikvold, P. A.; Wieckovski, A. *J. Chem. Phys.* **1996**, *104*, 5699.
(11) Toney, M. F.; Howard, J. N.; Richer, J.; Borges, G. L.; Gordon, J. G.; Melroy, O. R. *Phys. Rev. Lett.* **1995**, *75*, 4472.
(12) Omar, I. H.; Pauling, H. J.; Jüttner, K. *J. Electrochem. Soc.* **1983**, *140*, 2187.
(13) Mrozek, P.; Han, M.; Sung, Y.-E.; Wieckovski, A. *Surf. Sci.* **1994**, *319*, 21.
(14) Shi, Z.; Lipkowski, J. *J. Electroanal. Chem.* **1994**, *364*, 289.
(15) Magnussen, O. M.; Hagebock, J.; Hotlos, J.; Behm, R. J. *Faraday Discuss.* **1992**, *94*, 329.
(16) Batina, N.; Will, T.; Kolb, D. M. *Faraday Discuss.* **1992**, *94*, 93.

(17) Hotlos, J.; Magnussen, O. M.; Behm, R. J. *Surf. Sci.* **1995**, *335*, 129.
(18) Inukai, J.; Osawa, Y.; Wakisaka, M.; Sashikata, K.; Kim, Y. G.; Itaya, K. *J. Phys. Chem.* **1998**, *102*, 3498.
(19) Huang, L.; Zeppenfeld, P.; Horch, S.; Comsa, G. *J. Chem. Phys.* **1997**, *107* (2), 585.
(20) Wu, S.; Shi, Z.; Hitchcock, A. P.; Tyliszczak, T.; Lipkowski, J. *J. Phys. Chem. B* **1997**, *101*, 10310.
(21) **)** Tao, N. J.; Lindsay, S. M. *J. Phys. Chem.* **1992**, *96*, 5213.
(22) Gao, X.; Weaver, M. J. *J. Am. Chem. Soc.* **1992**, *114*, 8544.
(23) Sugita, S.; Abe, T.; Itaya, K. *J. Phys. Chem.* **1993**, *97*, 8780.
(24) McCarley, R. L.; Bard, A. *J. Phys. Chem.* **1992**, *95*, 9618.
(25) Matsumoto, H.; Oda, I.; Inukai, J.; Ito, M. *J. Electroanal. Chem.* **1993**, *356*, 275.
(26) Ocko, B. M.; Watson, G. M.; Wang, J. *J. Phys. Chem.* **1994**, *98*, 897.
(27) Martínez-Ruiz, A.; Valenzuela-Benavides, J.; Morales de la Garza, L.; Batina, N. *Surf. Sci.* **2001**, *476*, 139.
(28) Yamada, T.; Batina, N.; Itaya, K. *J. Phys. Chem.* **1995**, *99*, 8817.
(29) Yamada, T.; Batina, N.; Itaya, K. *Surf. Sci.* **1995**, *335*, 204.
(30) Yamada, T.; Ogaki, K.; Okubo, S.; Itaya, K. *Surf. Sci.* **1996**, *369*, 321.
(31) Batina, N.; Yamada, T.; Itaya, K. *Langmuir* **1995**, *11*, 4568.
(32) Bosco, E.; Rangaranjan, S. K. *J. Chem. Soc., Faraday Trans.* **1981**, *77*, 1673.
(33) Bewick, A.; Thomas, B. *J. Electroanal. Chem.* **1977**, *84*, 127.
(34) Bewick, A.; Thomas, B. *J. Electroanal. Chem.* **1977**, *85*, 329.
(35) Bewick, A.; Fleishmann, M.; Thirsk, H. R. *Trans. Faraday. Soc.* **1962**, *58*, 2200.
(36) Gibson, N. C.; Saville, P. M.; Harrington, D. A. *J. Electroanal. Chem.* **1991**, *318*, 271.
(37) Hölzle, M. H.; Zwing, V.; Kolb, D. M. *Electrochim. Acta* **1995**, *40*, 1237.
(38) Hölzle, M. H.; Retter, U.; Kolb, D. M. *J. Electroanal. Chem.* **1994**, *371*, 101.
(39) Hölzle, M. H.; Apsel, C. W.; Will, T.; Kolb, D. M. *J. Electrochem. Soc.* **1995**, *142*, 3741.
(40) Palomar-Pardavé, M.; Batina, N.; González, I. *J. Phys. Chem. B* **2000**, *104*, 3545.
(41) Palomar-Pardavé, M.; Miranda-Hernández, M.; Batina, N.; González, I. *J. Electroanal. Chem.* **1998**, *443*, 81.
(42) Palomar-Pardavé, M.; Miranda-Hernández, M.; Batina, N.; González, I. *Surf. Sci.* **1998**, *399*, 80.
(43) Magnusen, O. M.; Hotlos, J.; Nichols, R. J.; Kolb, D. M. *Phys. Rev. Lett.* **1990**, *63*, 2929.
(44) Jovicévić, J. N.; Jović, V. D.; Despić, A. R. *Electrochim. Acta* **1984**, *29*, 1625.
(45) *Adv. Electrochem. Electrochem. Eng.* **1993**, *3*, 123.
(46) Noel, M.; Vasu, K. *Cyclic Voltametry and the Frontiers of Electrochemistry*; Aspect: London, 1990; Chapter 7.
(47) Mendoza-Huizar, L. H.; Robles, J.; Palomar-Pardavé, M. *J. Electroanal. Chem.* **2002**, *521*, 95.